Wave-like properties of solar supergranulation

L. Gizon*, T. L. Duvall Jr† & J. Schou*

** W. W. Hansen Experimental Physics Laboratory, Stanford University, Stanford, California 94305, USA*
† Laboratory for Astronomy and Solar Physics, NASA Goddard Space Flight Center, Greenbelt, Maryland 20771, USA

Supergranulation[1,2] on the surface of the Sun is a pattern of horizontal outflows, outlined by a network of small magnetic features, with a distinct scale of 30 million metres and an apparent lifetime of one day. It is generally believed that supergranulation corresponds to a preferred 'cellular' scale of thermal convection; rising magnetic fields are dragged by the outflows and concentrated into 'ropes' at the 'cell' boundaries[3]. But as the convection zone is highly turbulent and stratified, numerical modelling has proved to be difficult and the dynamics remain poorly understood. Moreover, there is as yet no explanation for the observation that the pattern appears[4,5] to rotate faster around the Sun than the magnetic features. Here we report observations showing that supergranulation undergoes oscillations and supports waves with periods of 6–9 days. The waves are predominantly prograde, which explains the apparent super-rotation of the pattern. The rotation of the plasma through which the pattern propagates is consistent with the motion of the magnetic network.

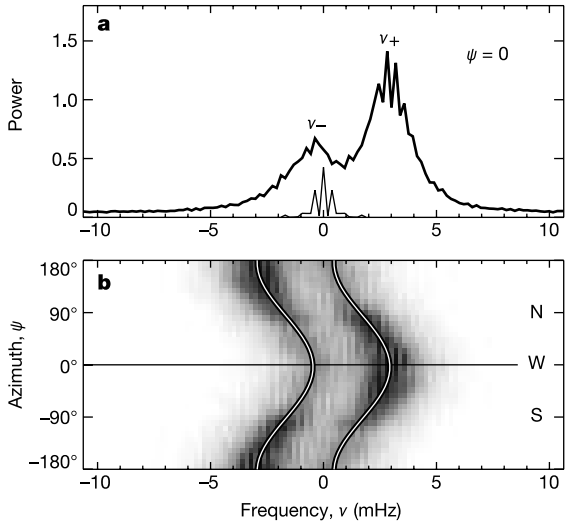

Figure 1 Power spectrum of the supergranulation signal near the solar equator ($\lambda = 0°$). Sections are shown at constant wavenumber $k = 120/R$, where R is the solar radius. **a**, The thick line is the power spectrum versus frequency, ν, for $\mathbf{k} = (k, 0)$ pointing in the direction of solar rotation, $\psi = 0$ (that is, west). There are two peaks, at frequencies ν_- and ν_+. The frequency resolution is given by the power spectrum of the temporal window function (thin line). **b**, Cylindrical section, $P_k(\nu,\psi)$, of the power spectrum at constant k, plotted against ν and the direction of $\mathbf{k}$, ψ. By construction, $P_k(\nu, \psi) = P_k(-\nu, \psi - \pi)$. Power peaks in two ridges at frequencies $\nu_-(\psi)$ and $\nu_+(\psi)$. For each ψ, we measure $\nu_\pm$ by fitting the sum of two independent lorentzian functions to the power. The fits take into account the convolution by the window function. The sinusoidal variation of $\nu_\pm$ with ψ is due to advection by a background flow $\mathbf{u} = (u_x, u_y)$. The double lines show the fit $\nu = \pm\nu_0 + (ku_x \cos\psi + ku_y \sin\psi)/2\pi$ to $\nu_\pm(\psi)$, where ν_0 is a constant frequency. At the equator we find $\mathbf{u} = (43, 0)\,\mathrm{m\,s^{-1}}$. The velocity u_x is measured in a frame co-rotating with the Sun at the Carrington rotation rate.

To study supergranulation, we use a 60-day sequence of Doppler velocity images obtained in 1996 by the Michelson Doppler Imager[6] (MDI) on board the Solar and Heliospheric Observatory (SOHO). Images are tracked at the Carrington angular velocity ($\Omega_C = 2.87\,\mu\mathrm{rad\,s^{-1}}$) to remove the main component of solar rotation. We apply the techniques of time-distance helioseismology[7] to obtain every 12 h a 120° × 120° map of the horizontal divergence of the flows in a 1-Mm-deep layer beneath the surface[8]. Unlike raw Doppler images, the divergence signal has uniform sensitivity across the solar disk and is subject to few systematic errors. Supergranules appear as cellular patterns of horizontal outward flow in the divergence maps.

For any given target latitude, λ, we extract a longitudinal section of the data 10°-wide in latitude centred about λ. The divergence signal is Fourier-transformed in three dimensions to make power spectra as a function of frequency, ν, and horizontal wavevector, $\mathbf{k} = (k_x, k_y)$, where k_x and k_y are in the east–west and south–north directions, respectively. In cylindrical coordinates, $\mathbf{k}$ is uniquely specified by its magnitude, k, and its direction, ψ, such that $k_x = k\cos\psi$ and $k_y = k\sin\psi$. Fig. 1 shows sections of the equatorial power spectrum at a constant k typical of the supergranulation. For each azimuth ψ, the power has two broad peaks at frequencies ν_+ and ν_- (Fig. 1a). No galilean transformation can cause these peaks to coalesce, at zero frequency or otherwise. This implies that the supergranulation undergoes oscillations.

Observations show that the frequencies $\nu_\pm$ have a sinusoidal dependence, with ψ of the form $\pm\nu_0 + \nu_1\cos(\psi - \psi_0)$ (Fig. 1b). We interpret ν_1 to be a Doppler frequency shift, $\nu_1 = k\|\mathbf{u}\|/2\pi$, produced by a horizontal background flow $\mathbf{u}$ with magnitude $\|\mathbf{u}\|$ and pointing in the direction ψ_0, as in helioseismological ring analysis[9]. The nearly linear relationship measured between ν_1 and k in the range $40 < kR < 180$, where R is the solar radius, is consistent with this interpretation. The latitudinal dependence of $\mathbf{u}$ is shown in Fig. 2. The inferred rotation (Fig. 2a) and meridional circulation (Fig. 2b) are both remarkably similar to that of the small magnetic features[10,11]. This property is consistent with the view that magnetic fields are advected by supergranular flows.

The dynamics of the supergranulation is best studied once the background flow, $\mathbf{u}$, has been removed. In a co-moving frame, each spatial component oscillates at a characteristic frequency ν_0. We find a clear relationship between ν_0 and the wavenumber k, well described by a power law (Fig. 3a). This is a fundamental relationship, as it is measured to be independent of both ψ and λ. The data are consistent with a spectrum of travelling waves with a dispersion

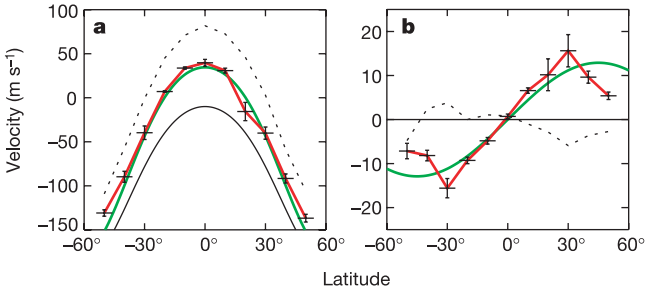

Figure 2 Flows, $\mathbf{u}$, inferred from the advection of the supergranulation, plotted against latitude, λ. **a**, Flow in the direction of solar rotation, u_x (red). The green line shows the rotation of the small magnetic features[10], and the black line is for the photospheric rotation[5]. The dotted line shows the pattern rotation obtained by tracking supergranular features with a 24-h delay, in agreement with an earlier measurement[5]. **b**, Northward meridional flow, u_y (red). The meridional flow of the magnetic features[11] (green) is again similar. The dotted line shows the anomalous results obtained by tracking the supergranulation pattern with a 24-h delay.

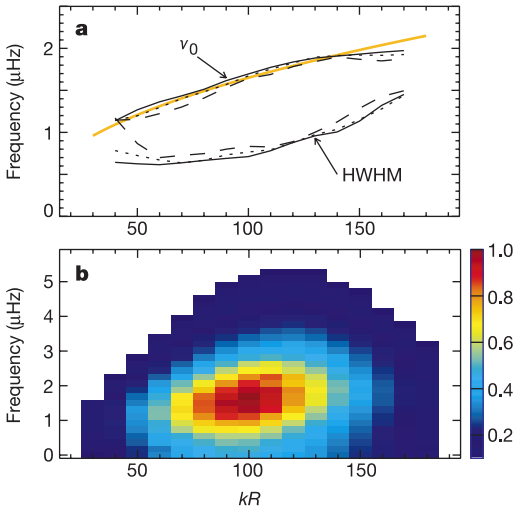

Figure 3 Average dynamical properties in a co-moving frame. **a**, Oscillation frequency ν_0 versus kR at latitudes $\lambda = 0°$ (solid), $\lambda = \pm 25°$ (dotted) and $\lambda = \pm 50°$ (dashed). For reference, we plot the approximate dispersion relation $\nu = 1.65(kR/100)^{0.45}$ μHz (orange). Also shown is the half-width at half-maximum (HWHM) of the lorentzian profiles for the same latitudes, implying an e-folding lifetime of 1–3 d. The quality factor, ν_0/HWHM, does not exceed 2. **b**, Power spectrum corrected for rotation and meridional circulation and averaged over azimuth and latitude. We note that the distribution of power as a function of frequency is affected only by the known temporal window function, whereas the wavenumber dependence includes effects of the telescope optics and of the time-distance analysis which are not fully understood.

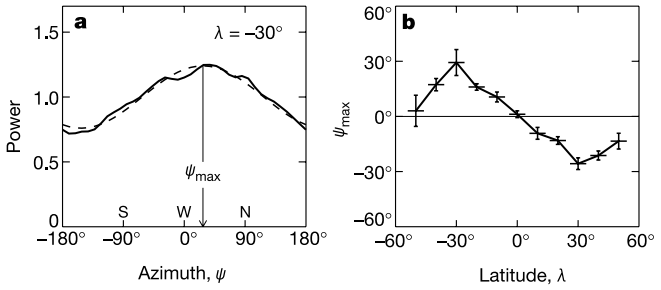

Figure 4 Wave power as a function of azimuth and latitude. **a**, Directional distribution of power at latitude $\lambda = -30°$ (solid line), obtained by integrating $P_k(\nu, \psi)$ over frequencies $\nu > \mathbf{k}\cdot\mathbf{u}/2\pi$ and then averaging over k. We applied an astigmatism correction estimated from the data. The azimuth of maximum power, ψ_{max}, is measured by fitting a sinusoidal function (dashed line). **b**, Plot of ψ_{max} versus latitude.

relation $\nu = \nu_0(k)$. The waves have a rather low quality factor, as can be seen in the azimuthally averaged power spectrum (Fig. 3b).

As ν_0 and the dominant size[12] of supergranules are observed to be essentially independent of latitude, the general dynamics determining the timescale and the spatial scale of supergranulation are not affected by the Coriolis force associated with the large-scale vorticity (rotation). We observe, however, a pronounced anisotropy in the azimuthal distribution of wave power at fixed k (Fig. 4a). The power is maximum in the direction of rotation and towards the equator in both hemispheres (Fig. 4b). The pattern therefore senses the effect of rotation. A snapshot of the divergence field would not reveal this, as the sum of the powers measured in opposite directions is isotropic (Fig. 4a); the vorticity field, on the other hand, is known[8] to be slightly sensitive to the effect of the Coriolis force.

Earlier estimates[4,5] of the supergranulation rotation, obtained by tracking the supergranulation pattern from one image to the next, were systematically found to be higher[13] than the rotation of the magnetic network (Fig. 2a). This apparent super-rotation of the pattern can now be understood, as waves are predominantly prograde. The east–west motion of the pattern is effectively a power-weighted average of the true rotation and the non-advective phase speed $u_w = 2\pi\nu_0/k \approx 65\,\mathrm{m\,s^{-1}}$. Similarly, the excess of wave power towards the equator is reflected in the meridional motion of the pattern (Fig. 2b).

We have shown that supergranulation displays a high level of organization in space and time. It is known[14] that heat and momentum transport in turbulent rotating convection is controlled by a network of coherent cyclonic plumes sinking from the thermal boundary layer. These plumes may be at the origin of the organization of the supergranulation pattern. We find that supergranulation supports waves. The prograde excess of wave power is probably due to the influence of rotation that breaks the east–west symmetry, allowing new instabilities to propagate. Recent numerical simulations[15] of solar convection show convective patterns that move prograde relative to the local rotation at low latitudes, and may help explain the observations. Convection in oblique magnetic fields[16] also exhibits solutions that take the form of travelling waves, where the tilt of the convection cells, their wave speed, and direction depend on the strength and obliquity of the field. Supergranulation appears to be a rare example of travelling wave convection in a very highly turbulent fluid, a nonlinear phenomenon that has been observed in laboratory experiments and numerical simulations[15–18] under conditions of much weaker turbulence. We suggest that supergranular waves may be used as a diagnostic tool for probing the upper solar convection zone. □

Received 2 May; accepted 29 October 2002; doi:10.1038/nature01287.

1. Leighton, R. B., Noyes, R. W. & Simon, G. W. Velocity fields in the solar atmosphere. I. Preliminary report. *Astrophys. J.* **135,** 474–499 (1962).
2. Simon, G. W. & Leighton, R. B. Velocity fields in the solar atmosphere. III. Large-scale motions, the chromospheric network, and magnetic fields. *Astrophys. J.* **140,** 1120–1147 (1964).
3. Galloway, D. J. & Weiss, N. O. Convection and magnetic fields in stars. *Astrophys. J.* **243,** 945–953 (1981).
4. Duvall, T. L. Jr The equatorial rotation rate of the supergranulation cells. *Sol. Phys.* **66,** 213–221 (1980).
5. Snodgrass, H. B. & Ulrich, R. K. Rotation of Doppler features in the solar photosphere. *Astrophys. J.* **351,** 309–316 (1990).
6. Scherrer, P. H. *et al.* The solar oscillations investigation—Michelson Doppler imager. *Sol. Phys.* **162,** 129–188 (1995).
7. Duvall, T. L. Jr *et al.* Time-distance helioseismology. *Nature* **362,** 430–432 (1993).
8. Duvall, T. L. Jr & Gizon, L. Time-distance helioseismology with f modes as a method for measurement of near-surface flows. *Sol. Phys.* **192,** 177–191 (2000).
9. Schou, J. & Bogart, R. S. Flow and horizontal displacements from ring diagrams. *Astrophys. J.* **504,** L131–L134 (1998).
10. Komm, R. W., Howard, R. F. & Harvey, J. W. Rotation rates of small magnetic features from two- and one-dimensional cross-correlation analyses. *Sol. Phys.* **145,** 1–10 (1993).
11. Komm, R. W., Howard, R. F. & Harvey, J. W. Meridional flow of small photospheric magnetic features. *Sol. Phys.* **147,** 207–223 (1993).
12. Beck, J. G. *Large Scale Solar Velocities on Time Scales up to Thirty Days.* Thesis, Univ. California (1997).
13. Beck, J. G. & Schou, J. Supergranulation rotation. *Sol. Phys.* **193,** 333–343 (2000).
14. Brummell, N. H., Hurlburt, N. E. & Toomre, J. Turbulent compressible convection with rotation. I. Flow structure and evolution. *Astrophys. J.* **473,** 494–513 (1996).
15. Miesch, M. S. *et al.* Three-dimensional spherical simulations of solar convection. I. Differential rotation and pattern evolution achieved with laminar and turbulent states. *Astrophys. J.* **532,** 593–615 (2000).
16. Hurlburt, N. E., Matthews, P. C. & Proctor, M. R. E. Nonlinear compressible convection in oblique magnetic fields. *Astrophys. J.* **457,** 933–938 (1996).
17. Zhong, F., Ecke, R. & Steinberg, V. Asymmetric modes and the transition to vortex structures in rotating Rayleigh-Bénard convection. *Phys. Rev. Lett.* **67,** 2473–2476 (1991).
18. Walden, R. W. *et al.* Traveling waves and chaos in convection in binary fluid mixtures. *Phys. Rev. Lett.* **55,** 496–499 (1985).

Acknowledgements We thank D. O. Gough for suggestions about the general presentation of this Letter, and P. Milford, P. H. Scherrer, C. J. Schrijver and N. O. Weiss for comments. SOHO is a mission of international cooperation between the European Space Agency and NASA. MDI is supported by the Office of Space Sciences of NASA.

Competing interests statement The authors declare that they have no competing financial interests.

Correspondence and requests for material should be addressed to L.G. (e-mail: lgizon@solar.stanford.edu).

24. Pan, T., Loria, A. & Zhong, K. Probing of tertiary interactions in RNA: 2′-hydroxyl-base contacts between the RNase P RNA and pre-tRNA. *Proc. Natl Acad. Sci. USA* **92,** 12510–12514 (1995).
25. Loria, A. & Pan, T. Recognition of the T stem-loop of a pre-tRNA substrate by the ribozyme from *Bacillus subtilis* ribonuclease P. *Biochemistry* **36,** 6317–6325 (1997).
26. Nolan, J. M., Burke, D. H. & Pace, N. R. Circularly permuted tRNAs as specific photoaffinity probes of ribonuclease P RNA structure. *Science* **261,** 762–765 (1993).
27. Hendrickson, W. A. Determination of macromolecular structures from anomalous diffraction of synchrotron radiation. *Science* **254,** 51–58 (1991).
28. Murshudov, G. N., Vagin, A. A. & Dodson, E. J. Refinement of macromolecular structures by the maximum-likelihood method. *Acta Crystallogr. D* **53,** 240–255 (1997).
29. Brunger, A. T. *et al.* Crystallography & NMR system: a new software suite for macromolecular structure determination. *Acta Crystallogr. D* **54,** 905–921 (1998).
30. Haas, E. S., Banta, A. B., Harris, J. K., Pace, N. R. & Brown, J. W. Structure and evolution of ribonuclease P RNA in Gram-positive bacteria. *Nucleic Acids Res.* **24,** 4775–4782 (1996).

Supplementary Information accompanies the paper on *Nature*'s website (http://www.nature.com/nature).

Acknowledgements We thank X. Liu and Y. Xiao for technical assistance, A. Changela, H. Feinberg, V. Grum and members of DND–CAT for help with data collection, and A. Changela, C. Correll, V. Grum, E. Sontheimer, B. Taneja and J. Wedekind for comments and suggestions. Research was supported by the NIH (to A.M.) and an NIH NRSA Fellowship to A.K. Support from the R.H. Lurie Cancer Center of Northwestern University to the Structural Biology Center is acknowledged. Portions of this work were performed at the DuPont–Northwestern–Dow Collaborative Access Team (DND–CAT) Synchrotron Research Center at the Advanced Photon Source (APS) and at the Stanford Synchrotron Radiation Laboratory (SSRL). DND–CAT is supported by DuPont, Dow and the NSF, and use of the APS is supported by the DOE. SSRL is operated by the DOE, Office of Basic Energy Sciences. The SSRL Biotechnology Program is supported by the NIH and the DOE.

Competing interests statement The authors declare that they have no competing financial interests.

Correspondence and requests for materials should be addressed to A.M. (e-mail: a-mondragon@northwestern.edu). Coordinates have been deposited in the Protein Data Bank under the accession code 1NBS.

retractions

A cytosolic catalase is needed to extend adult lifespan in *C. elegans daf-C* and *clk-1* mutants

J. Taub, J. F. Lau, C. Ma, J. H. Hahn, R. Hoque, J. Rothblatt & M. Chalfie

Nature **399**, 162–166 (1999).

We no longer have confidence in our observations associating a reduction in adult lifespan with a putative mutation in the *Caenorhabditis elegans* catalase gene *ctl-1* and therefore retract this paper. With the assistance of J. Liang and C. Keller, we have confirmed that *C. elegans* has multiple catalase genes (actually three in tandem) and that the original strain, TU1061, has decreased transcription of *ctl-1* messenger RNA. However, we have also found several errors, one identifying a single nucleotide deletion as the defect in the putative *ctl-1* mutation and others in the identification of strains carrying mutations in multiple genes. In particular, we have not seen the expected reduction in *ctl-1* mRNA in other strains tested. The longevity results obtained with these strains are therefore meaningless. We are grateful to our colleagues, particularly C. Kenyon and M. Crowder, for conveying to us their concerns about our results. □

Metal–insulator transition in chains with correlated disorder

Pedro Carpena, Pedro Bernaola-Galván, Plamen Ch. Ivanov & H. Eugene Stanley

Nature **418**, 955–959 (2002).

This Letter reported numerical simulations of one-dimensional disordered binary systems, and found a threshold value for the exponent characterizing the long-range power-law correlations of the system. Below this threshold, the system behaves as an insulator and above it, in the thermodynamic limit, the system behaves as a conductor. Unfortunately, we have now found that this observation was a consequence of the algorithm used to generate long-range correlations in binary chains, because above the threshold value of the exponent only a finite number of segments of atoms of the same type (A or B) exists, even in the thermodynamic limit of an infinitely large system. Thus, the system studied was not truly disordered. As a result, what we observed at the critical threshold value for the correlation exponent was not a transition from insulator to metal behaviour in a disordered system (as reported), but a transition from a disordered to an ordered system. For this reason, the authors retract the claim of a metal–insulator transition in the infinite binary chain with correlated disorder. The results are still valid that relate to the behaviour of a binary chain below the critical threshold value of the correlation exponent, and to large but finite system sizes (as found in the DNA example discussed in the Letter).

We thank L. Hufnagel and T. Geisel for drawing this to our attention. □

erratum

Wave-like properties of solar supergranulation

L. Gizon, T. L. Duvall Jr & J. Schou

Nature **421**, 43–44 (2003).

In Fig. 1, the units of frequency should be microhertz (μHz), not millihertz (mHz). In the US-printed issues, Fig. 3b appeared blurred. □

